NOTES AND CORRESPONDENCE

Sensible Heat Observations Reveal Soil-Water Evaporation Dynamics

J. L. HEITMAN

Department of Soil Science, North Carolina State University, Raleigh, North Carolina

R. HORTON

Department of Agronomy, Iowa State University, Ames, Iowa

T. J. SAUER

National Soil Tilth Laboratory, USDA-ARS, Ames, Iowa

T. M. DESUTTER

Department of Soil Science, North Dakota State University, Fargo, North Dakota

(Manuscript received 20 August 2007, in final form 27 November 2007)

ABSTRACT

Soil-water evaporation is important at scales ranging from microbial ecology to large-scale climate. Yet routine measurements are unable to capture rapidly shifting near-surface soil heat and water processes involved in soil-water evaporation. The objective of this study was to determine the depth and location of the evaporation zone within soil. Three-needle heat-pulse sensors were used to monitor soil heat capacity, thermal conductivity, and temperature below a bare soil surface in central Iowa during natural wetting/drying cycles. Soil heat flux and changes in heat storage were calculated from these data to obtain a balance of sensible heat components. The residual from this balance, attributed to latent heat from water vaporization, provides an estimate of in situ soil-water evaporation. As the soil dried following rainfall, results show divergence in the soil sensible heat flux with depth. Divergence in the heat flux indicates the location of a heat sink associated with soil-water evaporation. Evaporation estimates from the sensible heat balance provide depth and time patterns consistent with observed soil-water depletion patterns. Immediately after rainfall, evaporation occurred near the soil surface. Within 6 days after rainfall, the evaporation zone proceeded > 13 mm into the soil profile. Evaporation rates at the 3-mm depth reached peak values > 0.25 mm h^{-1}. Evaporation occurred simultaneously at multiple measured depth increments, but with time lag between peak evaporation rates for depths deeper below the soil surface. Implementation of finescale measurement techniques for the soil sensible heat balance provides a new opportunity to improve understanding of soil-water evaporation.

1. Introduction

Coupled heat and water processes occurring in shallow surface soil have inordinate impacts on terrestrial life, in particular soil-water evaporation and storage exert critical influences on land–atmosphere exchange of water and energy (Brubaker and Entekhabi 1996; D'Odorico et al. 2004). Early field experiments provided the first opportunity to observe temporal patterns in near-surface soil moisture and temperature (e.g., Jackson 1978). Since then, soil's role in land–atmosphere exchange has been parameterized in large-scale models (Sellers et al. 1997), often with limited appreciation for ubiquitous order-of-magnitude variations in hydrologic and thermal properties within the surface few centimeters of soil (Mahfouf and Noilhan 1991). Routine measurements are unable to capture rapidly

Corresponding author address: J. L. Heitman, Campus Box 7619, Department of Soil Science, North Carolina State University, Raleigh, NC 27695.
E-mail: jlheitman@ncsu.edu

DOI: 10.1175/2007JHM963.1

shifting near-surface soil heat and water processes despite their importance to understanding land surface hydrology (Entekhabi et al. 1999). Still, soil is so central to understanding land–atmosphere exchange that the 2007 Phoenix Mars Mission will include devices specifically designed to measure soil temperature, thermal properties, and water content (Cobos et al. 2006). Even with such far-reaching efforts, scientists have made no direct measurement of evaporative processes occurring within earth's terrestrial soil.

Researchers have long explored the connection between soil-water evaporation and soil heat flux (e.g., Gardner and Hanks 1966; Mayocchi and Bristow 1995). Unfortunately, inability to measure heat transfer at the finescale necessary to observe evaporative processes has limited investigation. Instead, the soil sensible heat flux is typically measured below the soil surface and a correction is made for the change in sensible heat storage above the flux measurement (e.g., Fuchs and Tanner 1968; Massman 1993). Latent heat is then accounted for at the plane of the soil surface, despite the moving depth of the evaporation front below the soil surface (de Vries and Philip 1986). Recent advances in the heat-pulse method for measuring soil thermal properties, sensible heat flux, and sensible heat storage (e.g., Ochsner et al. 2006, 2007) provide a new opportunity to investigate time and depth patterns of heat transfer and evaporation within soil. The objective of this study is to use finescale measurements of soil sensible heat to elucidate soil-water evaporation dynamics. Heat-pulse sensors installed under a bare soil surface measured soil sensible heat components during natural wetting/drying cycles. Soil-water evaporation is determined from the balance of the sensible heat components.

2. Methods

a. Soil sensible heat balance

Evaporation of soil water represents a large heat sink. A sensible heat balance is used to determine the amount of latent heat involved with vaporization of soil water following Gardner and Hanks (1966):

$$(H_0 - H_1) - \Delta S = LE, \tag{1}$$

where H_0 and H_1 are soil sensible heat fluxes (W m^{-2}) at depths 0 and 1, respectively; ΔS (W m^{-2}) is the change in soil sensible heat storage between depths 0 and 1; L (J m^{-3}) is the latent heat of vaporization; and E is evaporation (m s^{-1}). Using measurements of soil thermal conductivity (λ; W m^{-1} °C^{-1}) and the temperature gradient (dT/dz; °C, m^{-1}), values for H can be determined from Fourier's law (Ochsner et al. 2006). Ochsner et al. (2007) provide several approximations for determining ΔS from measured temperature (T; °C) and soil volumetric heat capacity (C; J m^{-3} °C^{-1}). In this study, we use

$$\Delta S = \sum_{i=1}^{N} C_{i,j-1} \frac{T_{i,j} - T_{i,j-1}}{t_j - t_{j-1}} (z_i - z_{i-1}), \tag{2}$$

where z (m) is depth and the subscripts i and j are index variables for depth layers and time steps, respectively.

The residual from the sensible heat balance provided by the left-hand side of Eq. (1) is attributed to LE, which cannot be measured directly. Values for L can be calculated from (Forsythe 1964)

$$L = 2.49463 \times 10^9 - 2.247 \times 10^6 \, T_m, \tag{3}$$

where T_m (°C) corresponds to the mean temperature for a given depth layer and time step. Having values for H, ΔS, and L it is possible to calculate E from Eq. (1).

b. Site description and instrumentation

Data for calculation of the heat balance were obtained from a bare surface field plot located in central Iowa (41°58′N, 93°41′W). The Koeppen climate classification for this region is Dfa (severe winter, no dry season, hot summer). Soil in the study area is Canisteo silty clay loam (fine-loamy, mixed, superactive, calcareous, mesic Typic Endoaquolls), which has nearly level relief and poor natural drainage. Experiments were conducted for a 40-day measurement period during late July to early September 2005. A 10 m × 10 m area selected for study was cleared of all vegetation and surface residue, and leveled.

Three-needle heat-pulse (HP) sensors identical to those described by Ren et al. (2003) were used in the experiments. The sensors consisted of three stainless steel needles (1.3-mm diameter, 4-cm length) fixed in parallel from an epoxy body, with adjacent needles spaced ≈ 6-mm apart. Each needle contained a 40-guage type E (chromel-constantan) thermocouple for measuring T. The central needle also contained a resistance heater for producing the slight heat input required for the HP method. The HP sensors were calibrated in agar stabilized water (6 g L^{-1}) both pre- and postdeployment to determine apparent needle spacing (Campbell et al. 1991).

Sensors were installed at 10 depths beginning immediately below the soil surface with the central needles of the sensors positioned at 6, 11, 16, 21, 26, 31, 36, 46, 56, and 66 mm. The plane formed by the three needles of each sensor was oriented perpendicular to the soil surface (Fig. 1). The sensors were connected to a data acquisition system on the soil surface. HP measurements were collected each 4 h for the duration of the study. The HP sequence for each sensor consisted of

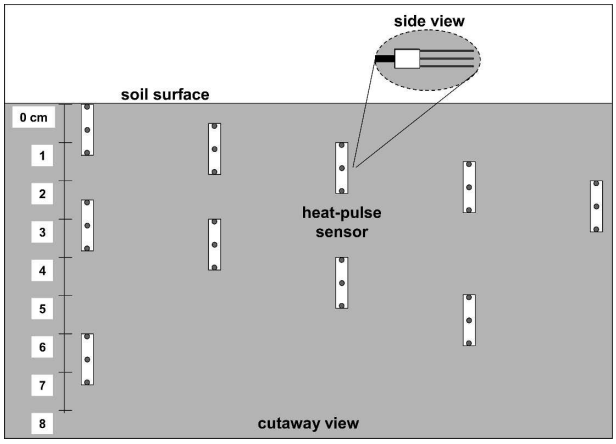

FIG. 1. Heat-pulse sensor arrangement. Ten sensors were installed in the upper 7.2 cm of the soil profile. The horizontal dimension is drawn to scale.

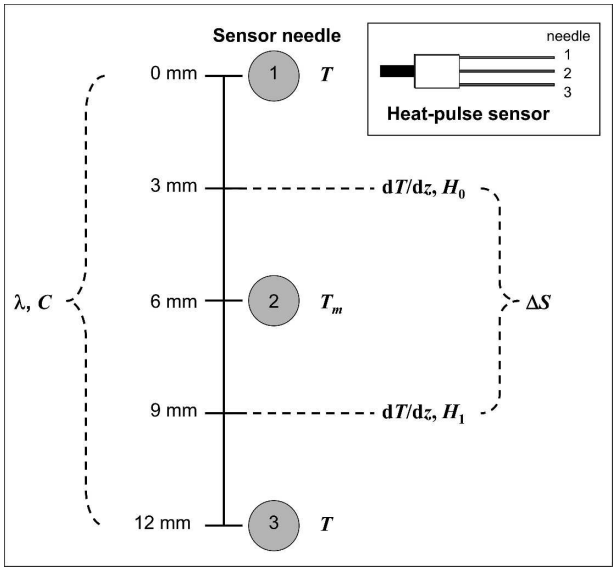

FIG. 2. Heat-pulse probe and measurement interpretation for heat balance calculation. Symbols denote thermal conductivity (λ), volumetric heat capacity (C), temperature (T), temperature gradient (dT/dz), soil heat flux (H_0 and H_1), and change in heat storage (ΔS).

30-s background temperature measurement (0.5-s measurement interval), 8-s heating of the central needle (≈30-J heat input), and measurement of the temperature response at the outer sensor needles for an additional 100 s. Soil volumetric heat capacity C and thermal diffusivity were determined from the heat input and temperature response following the procedures described by Knight and Kluitenberg (2004) and Bristow et al. (1994), respectively. The temperature response was corrected for ambient drift using the T measurements collected prior to HP initiation (Ochsner et al. 2006). Soil thermal conductivity λ was computed as the product of the thermal diffusivity and C. Thermocouples in each sensor needle were also used to record ambient soil T each 30 min (5-min average). Soil volumetric water content at each sensor depth was estimated from C (Ren et al. 2003; Heitman et al. 2003).

Net radiation at the soil surface was measured (30-min average) with a net radiometer (Mini Net Radiometer, Middleton and Co. Pty., Ltd., Melbourne, Australia) 10 cm above the soil surface. Soil surface T was measured with two high-precision infrared radiometric temperature (IRT) sensors (15° field of view; IRTS-P, Apogee Instruments, Inc., Logan, Utah) 1.5 m above the soil surface (30-min average), which were corrected for body temperature following Bugbee et al. (1998). Time centering of the measurement intervals was the same for the net radiometer, IRTs, and HP T. Soil volumetric water content in the upper 6 cm of the soil profile was also measured periodically following rainfall events with a portable theta probe (ML2, Delta-T Devices, Houston, Texas) using a calibration developed at the field site (Kaleita et al. 2005). Rainfall and air temperature (2-m height) were measured adjacent to the site.

c. Heat balance data handling

The sensor arrangement provided measurements of T, λ, and C from 0 to 72 mm (Fig. 1). Using these data, evaporation was estimated from Eq. (1) for each 1-h interval and for each ~6-mm depth increment [corresponding to calculation of Eq. (1) for each individual sensor] from 3 to 69 mm below the soil surface (Fig. 2). Hourly values for thermal properties were determined from time-weighted averaging of measurements collected each 4 h. Values for dT/dz were computed from the T difference between adjacent needles on a given sensor divided by the calibrated distance between the needles; dT/dz was assigned to the midpoint depth between the needles and computed as an average value for the 1-h time step. A single value for λ from the sensor was then multiplied with the respective dT/dz to compute H_0 and H_1 for each sensor. The change in heat storage ΔS [Eq. (2)] was computed from the 1-h T change at the middle needle of each sensor and measured C; ΔS was assumed to represent the depth increment between H_0 and H_1. An example calculation is shown in Table 1.

3. Results and discussion

a. Temporal conditions

The measurement period provided a range of evaporative conditions. Net radiation varied around rainfall

TABLE 1. Example soil heat balance calculation [Eq. (1)] for estimation of evaporation. Values are taken from measurements with a single sensor installed at the 16-mm depth for a 1-h time interval (1400 central standard time) on DOY 231. Variables are depth (z), temperature (T), thermal conductivity (λ), heat capacity (C), temperature gradient (dT/dz), heat flux (H), change in heat storage (ΔS), latent heat of vaporization (L), and evaporation (E).

Depth index	z (mm)	$T_{i,j-1}$[a] (°C)	$T_{i,j}$ (°C)	λ (W m^{-1} °C^{-1})	C (MJ m^{-3} °C^{-1})	dT/dz[b] (°C m^{-1})	H (W m^{-2})	ΔS[c] (W m^{-2})	L[c] (MJ m^{-3})	E[c] (mm h^{-1})
1	9.76	47.218	45.203							
	12.88					−254	267			
2	16	45.463	43.784	1.05	1.73			−4.9	2394	0.15
	19.21					−165	173			
3	22.41	44.258	42.871							

[a] Subscripts i and j refer to depth and time, respectively; the interval j-1 to j is 1 h.
[b] Computed based on the average temperatures for the 1-h interval.
[c] Values are assumed to represent the depth interval from 12.88 to 19.21 mm.

events, but maximum daily values typically approached 500 W m^{-2} (Fig. 3a). Mean daily maximum and minimum air T for the measurement period were 29.7° and 14.3°C, respectively (data not shown). Rainfall occurred on 10 days with five composite wetting/drying cycles. Periodic measurements of volumetric water content in the upper 6 cm of the soil (theta probe) indicate a range from 0.32 to 0.19 m^3 m^{-3} with rapid decreases from drainage and/or evaporation occurring within 2–3 days of rainfall events (Fig. 3b). Soil surface T (IRT) ranged between 55° and 10°C, while 6-cm soil temperature ranged between 41° and 16°C (Fig. 3c). Mean soil T was lowest during moist conditions, but T increased in daily mean and amplitude between rainfall events.

Soil thermal properties near the surface were influenced by wetting/drying cycles. Figure 4 shows depth-integrated λ and C from all HP sensors (3 to 72 mm). Both λ and C increase following rainfall events and decrease with subsequent drying. However, C decreases more dramatically immediately following each event, while decreases in λ tend to be slightly more gradual. Though both thermal properties are affected by changes in moisture, C is more linearly related to the volume fraction of water (de Vries 1963) and thereby changes more rapidly with water drainage following rainfall events; λ is less affected by the initial water loss. Compared to the initial changes in C, subsequent changes 2–3 days after rainfall events are less pronounced because significant liquid water redistribution is limited by soil hydraulic properties.

It is also notable that both thermal properties show evidence of diurnal cycling (Fig. 4). The time scale of thermal property measurements (each 4 h) prevents close examination of diurnal patterns, but thermal properties generally decreased from midmorning through afternoon and increased from late evening through early morning, which is consistent with diurnal cycling in near-surface soil water content observed by others (Rose 1968; Jackson 1978; Cahill and Parlange 1998). The observed diurnal variation was typically <8% of the daily mean value for both λ and C.

b. Divergence in the soil heat flux

Changes in soil temperature, water content, and thermal properties provide an indication of drying between rainfall events. To further examine this process we follow the progression of the soil heat flux and thermal conductivity during drying after a rainfall event. Data

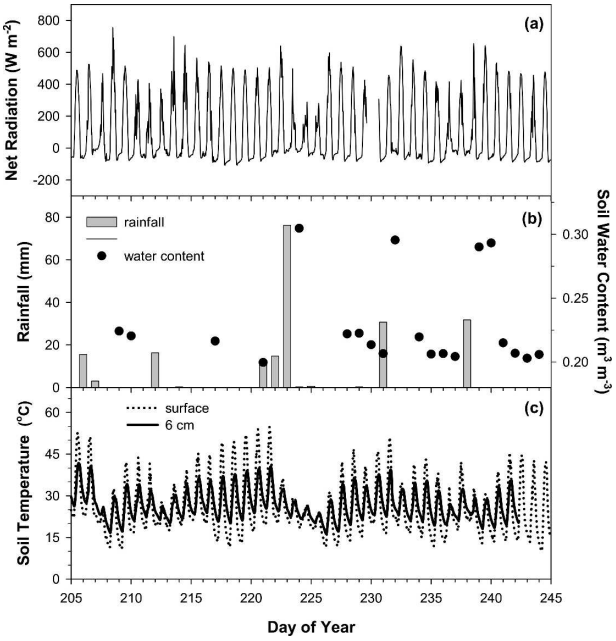

FIG. 3. Temporal conditions during the 40-day measurement period: (a) net radiation, (b) rainfall and soil volumetric water content, and (c) soil temperature. Labels on the x axis correspond to 00:00 central standard time for the days shown.

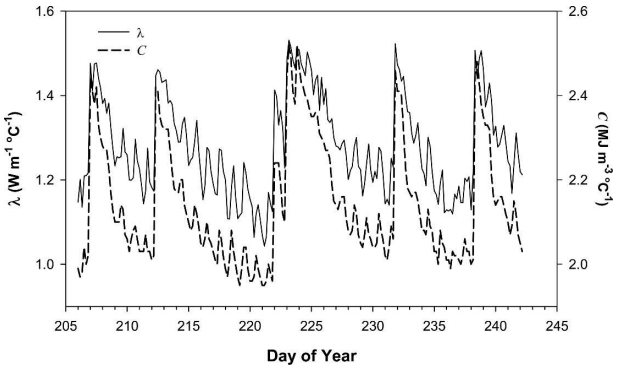

FIG. 4. Temporal patterns in soil thermal conductivity (λ) and volumetric heat capacity (C) for the 0–72-mm depth increment. Labels on the x axis correspond to 00:00 central standard time for the days shown.

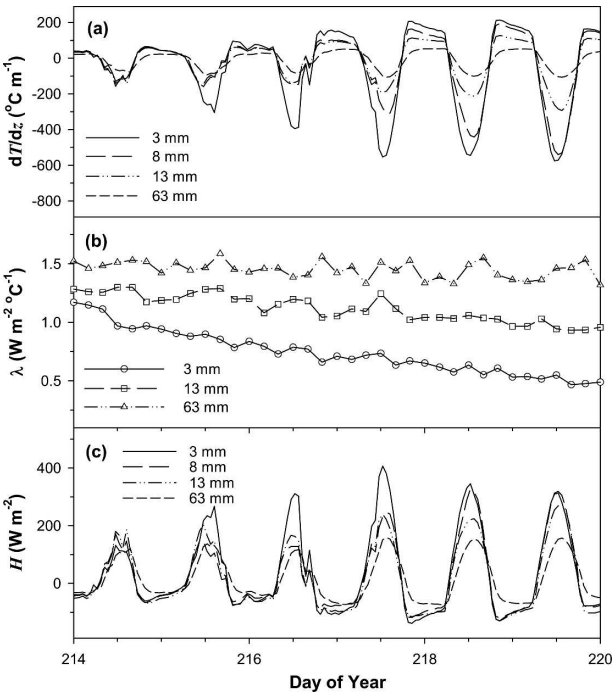

FIG. 5. Soil conditions following a rainfall event on DOY 212: (a) temperature gradient (dT/dz), (b) thermal conductivity (λ), and (c) sensible heat flux (H). Labels on the x axis correspond to 00:00 central standard time for the days shown. Symbols in (b) indicate measurements recorded each 4 h.

presented in the following sections represent a 6-day period with clear-sky conditions following a 20-mm rainfall on day of year (DOY) 212. A small (<2 mm) rainfall event occurred on DOY 214.

Temperature gradients drive soil sensible heat transfer. Measurements at four subsurface depths indicate temporal changes in temperature gradients after rainfall on DOY 212 (Fig. 5a). Immediately following rainfall, when soil conditions are relatively moist and thermal properties are near uniform, temperature gradients differ only slightly with depth (DOY 214–215). However, as soil dries from the surface downward and air replaces water in pore spaces, λ decreases (Fig. 5b). As a dry soil zone propagates downward, temperature gradients begin to diverge (Fig. 5a).

Driven by temperature gradients, soil sensible heat flux varies only slightly with depth after rainfall (Fig. 5c). Heat flux begins to diverge at 3 mm on DOY 215, while deeper heat fluxes have similar amplitudes until DOY 217. Here, the maximum heat flux at 3 mm (>400 W m^{-2}) approaches 80% of net radiation (Fig. 3a). That the sensible heat flux represents such a large proportion of net radiation may be surprising. However, it must be recognized that the 3-mm sensible heat flux includes heat that is partitioned to latent heat deeper within the soil (Mayocchi and Bristow 1995). This heat flux is actually the sum of the traditional sensible soil heat flux and the latent heat flux. Divergence in heat fluxes between 3 and 8 mm is an important indicator of processes occurring between these depths. Soil heat flux is often reported by accounting for latent heat in the surface energy balance. However, direct measurement of the sensible heat flux divergence and the change in sensible heat storage provides a means to determine time and depth variation of soil-water evaporation by heat balance [i.e., Eq. (1)]. Taking into account the change in sensible heat storage, the divergence indicates a large heat sink associated with heat consumption for water vaporization.

c. *Soil-water evaporation and drying*

The rate and location of soil-water evaporation can be tracked using the heat-balance of Eq. (1). Immediately following rainfall, when soil water is not limiting, evaporation occurs at or near the soil surface; thus evaporation rates within the soil (i.e., 3 mm and deeper) are small (Fig. 6a). However, as the soil surface dries, there is a shift from atmospheric demand-controlled to soil-limited evaporation. Here this corresponds to DOY 215, where a significant decrease in water content (estimated from C) is evident at 3 mm (Fig. 6b). Thereafter, evaporation occurs deeper within the soil and the evaporation rate in the 3–8-mm soil layer begins to increase (Fig. 6a).

Peak evaporation rates occur at midday, but decline by late afternoon (Fig. 6a). Water content decreases from late morning through the afternoon and then increases from afternoon to late morning on the following day (Fig. 6b). This diurnal pattern derives from evaporation. Peak evaporation in the midday depletes shal-

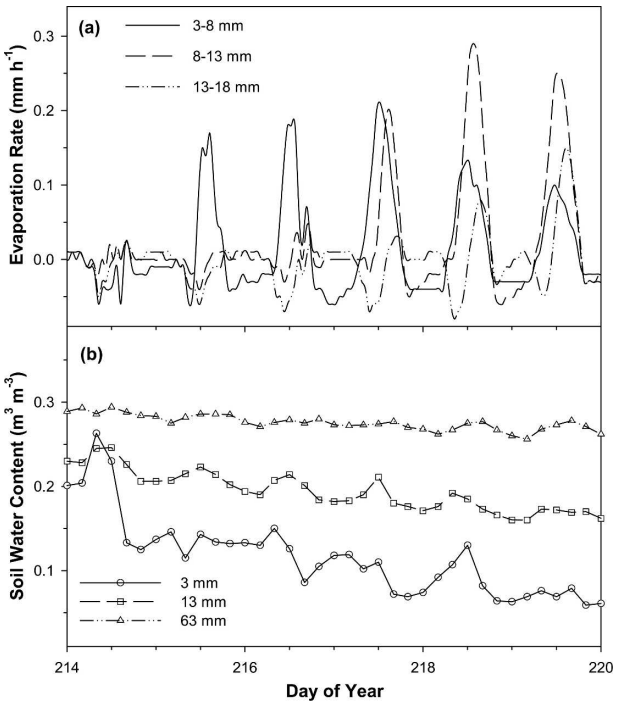

FIG. 6. Soil conditions following a rainfall event on DOY 212: (a) evaporation rate and (b) soil water content. Labels on the *x* axis correspond to 00:00 central standard time for the days shown. Symbols in (b) indicate measurements recorded each 4 h. Note that a minor short-duration rainfall event (<2 mm) temporarily increased water content at the 3-mm depth on DOY 214.

low soil water. As evaporation slows through evening, the dry surface soil rewets with water moving upward from below. This partially replenishes water depletion before evaporation begins on the following day. Eventually, as soil hydraulic conductivity decreases with drying, water redistribution and evaporation become soil-limited. As the surface soil continues to dry on subsequent days and the depth of the dry soil layer increases, the evaporation rate in the 8–13-mm layer begins to increase, eventually surpassing the declining evaporation rate in the soil layer above on DOY 217. By DOY 219, the evaporation rate in the 13–18-mm layer also surpasses the evaporation rate in the 3–8-mm layer.

These observations of evaporation suggest that evaporation occurs within a soil zone, rather than at a single depth plane. For example, on DOY 217 and 218, evaporation occurs simultaneously in both the 3–8- and 8–13-mm layers. This diffuse evaporation zone is consistent with the conceptual model of Yamanaka and Yonetani (1999), who describe the primary evaporation zone at the bottom of the dry surface soil layer, but with some evaporation still occurring in the dry soil above. While measurements here do not include evaporation occurring above the 3-mm soil depth, the relatively low composite evaporation rate from DOY 216 and 217 (when compared to DOY 218 and later) suggests that some evaporation is still occurring above 3 mm in the soil profile during this time period.

Also notable is the time lag for peak evaporation rates between depth increments (Fig. 6a). As might be expected from diurnal progression of heat transfer from the soil surface, daily peak evaporation for a given depth increment occurs earliest nearer to the soil surface. As heat propagates into the soil, evaporation rates deeper in the soil begin to increase. This pattern is consistent throughout the drying period, even as the peak magnitude of evaporation begins to decline in the 3–8-mm layer. Slightly negative values for the heat balance (i.e., $E < 0$) were also sometimes observed below the primary zone of evaporation. This may be an artifact of measurement error. In particular, uncertainty in depth resolution between the points of temperature observation is critical, because it affects both the magnitude of heat flux (via temperature gradient) and heat storage (via depth increment) terms. However, negative values for the heat balance may also suggest condensation. With evaporation, water vapor moves out of the soil, but some vapor may also move deeper into the soil profile through diffusion (Grifoll et al. 2005). Given that conditions are cooler below 3 mm, condensation of this water vapor may occur, which appears at least consistent with the pattern observed here. Further evaluation of the heat balance method is warranted to quantify this mechanism.

Measurements of finescale soil sensible heat and the heat balance provide a new opportunity to observe the process of soil-water evaporation. Throughout drying, progression and shifting of the soil-water evaporation zone is apparent (Fig. 6a). Energy partitioning and the soil heat flux (Fig. 5c) are influenced by soil properties that change with drying (Fig. 5b). Energy partitioned to latent heat with water vaporization, in turn, influences soil moisture and the supply of water for further evaporation (Fig. 6b).

4. Summary and conclusions

Transient soil-water evaporation impacts the natural environment from the scale of the soil microbial communities to large-scale weather patterns. Yet, the dynamic processes involved in soil-water evaporation have not been fully observed or measured. Instead evaporation is typically assigned to the surface energy balance without considering the direct influences of soil mechanisms. The objective of this work is to demonstrate the evaporative process occurring within soil. Here, heat-pulse sensors were used to measure soil

thermal properties and temperature for multiple depth increments. These finescale measurements show divergence in the near-surface sensible heat flux during drying. By accounting for the change in sensible heat storage through measurement, it is demonstrated that the divergence largely represents evaporation occurring within the soil. Patterns in soil thermal conductivity, temperature gradient, soil heat flux, evaporation, and water content show internal consistency. Observations reveal shifts in the magnitude and location of evaporation as the soil dries after rainfall. Heat flux near the soil surface represents a large fraction of net radiation, here as much as 80%, as the evaporation zone proceeds downward and near-surface soil-water is depleted. Implementation of finescale techniques for the measurement of soil sensible heat balance provides a new opportunity to improve understanding of evaporation dynamics and soil heat transfer in the study of a wide range of environmental interactions. The connection between soil heat transfer and evaporation in land–atmosphere exchange should also be considered in the development of mechanistic land surface models and large-scale measurement efforts.

Acknowledgments. This journal paper of the Iowa Agricultural and Home Economics Experiment Station, Ames, Iowa, was supported by the National Science Foundation under Grant 0337533 and Hatch Act and State of Iowa funds. The authors gratefully acknowledge J. M. Norman for providing net radiometers for use in the experiments.

REFERENCES

Bristow, K. L., G. J. Kluitenberg, and R. Horton, 1994: Measurement of soil thermal properties with a dual-probe heat-pulse technique. *Soil Sci. Soc. Amer. J.,* **58,** 1288–1294.

Brubaker, K. L., and D. Entekhabi, 1996: Analysis of feedback mechanisms in land-atmosphere interaction. *Water Resour. Res.,* **5,** 1343–1357.

Bugbee, B., M. Droter, O. Monje, and B. Tanner, 1998: Evaluation and modification of commercial infra-red transducers for leaf temperature measurement. *Adv. Space Res.,* **10,** 1425–1434.

Cahill, A. T., and M. B. Parlange, 1998: On water vapor transport in field soils. *Water Resour. Res.,* **34,** 731–739.

Campbell, G. S., C. Calissendorff, and J. H. Williams, 1991: Probe for measuring soil specific heat using a heat-pulse method. *Soil Sci. Soc. Amer. J.,* **55,** 291–293.

Cobos, D. R., G. Campbell, and C. S. Campbell, 2006: Taking soil science to outer space: The thermal and electrical conductivity probe (TECP) for the Phoenix 2007 Scout Mission to Mars. *Extended Abstracts, 18th World Congress of Soil Science,* Philadelphia, PA, Soil Science Society of America, CD-ROM.

de Vries, D. A., 1963: Thermal properties of soils. *Physics of Plant Environment,* W. R. van Wijk, Ed., North Holland Publishers.

——, and J. R. Philip, 1986: Soil heat flux, thermal conductivity, and the null alignment method. *Soil Sci. Soc. Amer. J.,* **50,** 12–18.

D'Odorico, P., A. Porporato, and R. E. Dickinson, 2004: Preferential states in soil moisture and climate dynamics. *Proc. Natl. Acad. Sci.,* **101,** 8848–8851.

Entekhabi, D., and Coauthors, 1999: An agenda for land surface hydrology research and a call for the Second International Hydrological Decade. *Bull. Amer. Meteor. Soc.,* **80,** 2043–2058.

Forsythe, W. E., 1964: Smithsonian physical tables. Smithsonian Institution Publication 4169, Washington, DC.

Fuchs, M., and C. B. Tanner, 1968: Calibration and field test of soil heat flux plates. *Soil Sci. Soc. Amer. Proc.,* **32,** 326–328.

Gardner, H. R., and R. J. Hanks, 1966: Evaluation of the evaporation zone in soil by measurement of heat flux. *Soil Sci. Soc. Amer. Proc.,* **32,** 326–328.

Grifoll, J., J. M. Gasto, and Y. Cohen, 2005: Non-isothermal soil water transport and evaporation. *Adv. Water Resour.,* **28,** 1254–1266.

Heitman, J. L., J. M. Basinger, G. J. Kluitenberg, J. M. Ham, J. M. Frank, and P. L. Barnes, 2003: Field evaluation of the dual-probe heat-pulse method for measuring soil water content. *Vadose Zone J.,* **2,** 552–560.

Jackson, R. D., 1978: Diurnal changes in soil water content during drying. *Field Soil Water Regime,* R. Bruce, K. Flach, and H. Taylor, Eds., Soil Science Society of America, 37–76.

Kaleita, A., J. L. Heitman, and S. A. Logsdon, 2005: Field calibration of the theta probe for Des Moines lobe soils. *Appl. Eng. Agric.,* **21,** 865–870.

Knight, J. H., and G. J. Kluitenberg, 2004: Simplified computational approach for the dual-probe heat-pulse method. *Soil Sci. Soc. Amer. J.,* **68,** 447–449.

Mahfouf, J. F., and J. Noilhan, 1991: Comparative study of various formulations of evaporation from bare soil using in situ data. *J. Appl. Meteor.,* **30,** 1354–1365.

Massman, W. J., 1993: Errors associated with the combination method for estimating soil heat flux. *Soil Sci. Soc. Amer. J.,* **57,** 1198–1202.

Mayocchi, C. L., and K. L. Bristow, 1995: Soil surface heat flux: Some general questions and comments on measurements. *Agric. For. Meteor.,* **75,** 43–50.

Ochsner, T. E., T. J. Sauer, and R. Horton, 2006: Field tests of soil heat flux plates and some alternatives. *Agron. J.,* **98,** 1005–1014.

——, ——, and ——, 2007: Soil heat storage measurements in energy balance studies. *Agron. J.,* **99,** 311–319.

Ren, T., T. E. Ochsner, and R. Horton, 2003: Development of thermo-time domain reflectometry for vadose zone measurements. *Vadose Zone J.,* **2,** 544–551.

Rose, C. W., 1968: Water transport in soil with a daily temperature wave. I. Theory and experiment. *Aust. J. Soil Res.,* **6,** 31–44.

Sellers, P. J., and Coauthors, 1997: Modeling the exchange of energy, water, and carbon between continents and the atmosphere. *Science,* **275,** 502–509.

Yamanaka, T., and T. Yonetani, 1999: Dynamics of the evaporation zone in dry sandy soils. *J. Hydrol.,* **217,** 135–148.